ACS APPLIED MATERIALS & INTERFACES

Research Article

www.acsami.org

Newly Synthesized Silicon Quantum Dot–Polystyrene Nanocomposite Having Thermally Robust Positive Charge Trapping

Mai Xuan Dung, Jin-Kyu Choi, and Hyun-Dam Jeong*

Nanomaterials and Interface Laboratory, Department of Chemistry, Chonnam National University, 500-757 Gwangju, Republic of Korea

Supporting Information

ABSTRACT: Striving to replace the well known silicon nanocrystals embedded in oxides with solution-processable charge-trapping materials has been debated because of large scale and cost effective demands. Herein, a silicon quantum dot–polystyrene (SiQD–PS) nanocomposite (NC) was synthesized by post-functionalization of hydrogen-terminated silicon quantum dots (H-SiQDs) with styrene using a thermally induced surface-initiated polymerization approach. The NC contains two miscible components: PS and SiQD@PS which, respectively, are polystyrene and polystyrene chains-capped SiQDs. Spin-coated films of the nanocomposite on various substrate were thermally annealed at different temperatures and subsequently used to construct metal-insulator-semiconductor (MIS) devices and thin film field-effect transistors (TFTs) having a structure of p-Si^{++}/SiO_2/NC/pentacene/Au source-drain. Capacitance–voltage (C–V) curves obtained from the MIS devices exhibit a well-defined counterclockwise hysteresis with negative fat band shifts, which was stable over a wide range of curing temperatures (50–250 °C). The positive charge trapping capability of the NC originates from the spherical potential well structure of the SiQD@PS component while the strong chemical bonding between SiQDs and polystyrene chains accounts for the thermal stability of the charge trapping property. The transfer curve of the transistor was controllably shifted to the negative direction by varying applied gate voltage. Thereby, this newly synthesized and solution processable SiQD–PS nanocomposite is applicable as charge trapping materials for TFT based memory devices.

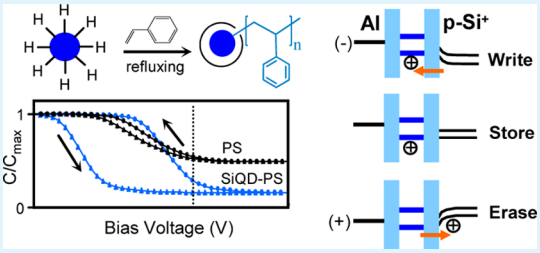

KEYWORDS: *silicon quantum dots, polystyrene, nanocomposite, C–V hysteresis, charge trapping memory, OTFTs*

1. INTRODUCTION

Since the first report by Tiwari[1] demonstrating the use of silicon nanocrystals to replace the polysilicon floating gate in nonvolatile memory devices, many other materials have been tested.[2−4] Among the nanocrystal-based memory devices, silicon nanocrystals embedded in SiO_2 have received much interest due to the perfect interface between the silicon nanocrystals and SiO_2.[5] The oxide matrix acts as a potential barrier that confines trapped charges within the individual silicon nanocrystals, thus reducing the charge loss due to interparticle tunneling or to leakage to the channel or gates.[1] Therefore, not only the nanocrystals, themselves, but also the insulating matrix and their interface quality are of importance to the device performance. Much of the effort to fabricate silicon nanocrystals embedded in an oxide insulating matrix has incorporated synthetic procedures that require either high temperatures and/or ultra high vacuum conditions, all of which are inappropriate for large scale processes or organic based electronics applications.[5,6] Several solution processes have been successfully established to fabricate memory devices in which pre-prepared or in-situ grown metal or semiconductor nanocrystals are embedded in a large bandgap polymer.[3,7−9] Striving to adopt these methods to fabricate silicon nanocrystal based nanocomposites, however, remains a big challenge, probably due to the difficulty in preparing stable colloidal silicon nanocrystals.[10] Additionally, the surface chemistry of colloidal silicon nanocrystals needs to be similar with that of the polymer host matrix in order to avoid the aggregation of nanocrystals during device fabrications.[11,12]

In many memory device configurations, polystyrene is frequently used as an insulating matrix because it has a large bandgap and high chemical and thermal stabilities, and it provides good insulator–organic semiconductor interfaces as well.[13−17] Therefore, to obtain a miscible silicon nanocrystals–polystyrene system by using pre-prepared colloidal silicon nanocrystals, one should not functionalize the silicon nanocrystals with a conventional monolayer of alkyl or alkoxide, the step needed to prevent the silicon nanocrystals from unwanted oxidation,[18,19] because the fatty alkyl chains have negligible dipolar and hydrogen bonding interactions compared with those of polystyrene.[12] Surface chemistry of silicon nanocrystals can be adjusted readily by a hydrosilylation reaction between hydrogen-terminated silicon nanocrystals, which are the most convenient intermediate to start with, and an appropriate alkene or alkyne.[20,21] A sub-monolayer of the capping molecule is formed on the surfaces of silicon nanocrystals through a Pt-

Received: September 27, 2012
Accepted: March 4, 2013
Published: March 19, 2013

 © 2013 American Chemical Society

catalyzed hydrosilylation,[21,22] while oligomer of the capping molecule can be formed and chemically bonds to the silicon nanocrystals if the reaction is initiated by UV light or by high temperatures owing to the formation of $Si^{\cdot}$ radical during the reaction course.[23−25] The surface initiated thermally-induced polymerization approach has been used widely to synthesize polymer coated inorganic nanoparticles, such as polystyrene-grafted TiO_2.[26]

Herein, we report a simple method to synthesize silicon quantum dot−polystyrene (SiQD−PS) nanocomposite (NC) by refluxing pre-prepared hydrogen-terminated SiQDs in styrene. The NC consists of two miscible components, polystyrene (PS) and SiQDs, that are capped by polystyrene chains (SiQD@PS) with an average diameter of 3.5 nm. Charge trapping properties of the NC were examined through metal-insulator-semiconductor (MIS) devices and Au/pentacen/charge trapping layer/SiO_2/p-Si^{++} transistors, all of which were constructed using pre-prepared thin films of NC spin-coated on corresponding substrates. The NC exhibited hole trapping ability, which was stable over a wide range of curing temperatures, 50−250 °C. These novel properties: solution processability, charge trapping ability, and thermal stability originate from the spherical potential well structure of the Si@PS component, in which a SiQD is capped by polystyrene chains. It is demonstrated that this newly synthesized SiQD−PS NC is applicable as a charge trapping material in organic field-effect transistor (OTFT) based nonvolatile memory devices. To the best of our knowledge, this report presents the first attempt to fabricate MIS and OTFT based memory devices using solution-processed thin films of a NC that contains SiQDs.

2. EXPERIMENTAL SECTION

Synthesis of SiQD−PS Nanocomposite. All chemicals were purchased from Aldrich and directly used without any purification steps. The synthesis procedure was carried out in Ar atmosphere using the Schlenk line technique. A solution of 0.6 mL of $SiCl_4$ in 300 mL of anhydrous toluene was sonicated for 90 min to form a miniemulsion system, which was then reduced to hydrogen-terminated silicon quantum dots (H-SiQDs) by adding slowly a 9 mL solution of $LiAlH_4$ (2M in THF). After 2 h of sonication, the remaining $LiAlH_4$ was quenched by 7 g of $CuSO_4$, and then, 3 mL of pre-distillated styrene monomer was added. The resultant mixture was refluxed for 12 h. To collect the NC, all solvents were removed under reduced pressure at 40 °C using a rotary evaporator. One hundred milliliters of anhydrous toluene was then added, and the resultant mixture was centrifuged at 15 000 (rotations per minute) for 10 min to remove the solid. The obtained solution was subsequently extracted with water (100 mL × 3 times), dried with brine (50 mL × 3 times), dried with 2 g of $MgSO_4$, and finally filtered through a 0.2 μm pore sized membrane to perform a transparent solution of the NC in toluene. The toluene solvent was evaporated, and the NC was further dried at 100 °C in a vacuum oven overnight. A control polystyrene sample, named as PS0, was also prepared using the same procedure as above, excluding the addition of $SiCl_4$. In order to explain more concretely the optical properties and morphology of thin films of SiQD−PS NC, octyl-capped Si QDs and phenethyl-capped SiQDs were also prepared using the above procedure with a modification that the capping step was carried out at room temperature by a Pt-catalyzed hydrosilylation approach, in which 0.3 mL of a Pt solution (0.05 M of H_2PtCl_6 in methanol) and 15 mL of 1-octene or styrene were added, respectively. This functionalization approach is known to perform a sub-monolayer of the capping molecule on the surface of SiQDs, and no polymerization reaction is expected.

Thin Film Fabrication. Substrates including quartz, p-Si^{+} wafer (with a resistivity of 1−30 Ω·cm and a thickness of 525 ± 25 μm), and thermally-oxidized p-Si^{++} silicon wafer (a 100 nm-thick SiO_2 layer on heavily doped p-type silicon wafer with a resistivity of <0.005 Ω·cm and a thickness of 525 ± 25 μm) were cleaned sequentially with methanol and acetone and finally dried by a nitrogen flow. Coating solutions with a concentration of 5 or 3 weight percentage (wt %) were prepared by dissolving the dried SiQD−PS NC (or the PS0) into a calculated amount of chlorobenzene solvent. The coating solutions were poured onto the substrates, which were then by spun at 2500 rotation per minute (rpm) for 25 seconds following a wetting step rotated at 500 rpm for 5 seconds. The films were then cured at different temperatures: 50, 100, 150, 200, 250, or 300 °C for 1 h under reduced pressure (10^{-2} Torr) in a tube vacuum furnace.

Device Fabrication. Thin films of the NC (or PS0) on p-Si^{+} substrates were used to fabricate metal-insulator-semiconductor (MIS) devices, in which the p-Si^{+} substrate serves as a semiconductor layer, in order to investigate the charge trapping property. Al electrodes with a diameter of about 0.55 mm and a thickness of about 300 nm were deposited on the top of the NC (or PSO) films by employing a stainless steel shadow mask. A thin layer of Al was also deposited on the backside of the p-Si^{+} substrate to minimize contact resistance. The depositions were carried out in a thermal deposition chamber with a working pressure of about 10^{-6} Torr.

To examine the applicability of the NC into charge trapping memory devices, three TFT devices having a structure of p-Si^{++}/SiO_2/ with or without a film of NC or PSO cured at 200 °C/pentacene/Au source-drain were constructed as follows. Thin films of the NC (or the PSO) with a thickness of about 50 nm on the thermally-oxidized silicon substrates (SiO_2/p-Si^{++}) served as substrates on which a pentacene layer with thickness of about 100 nm was thermally deposited at a rate of 0.75±0.25 Å/s using a thermal deposition chamber. During the deposition of pentacene, substrate temperature and working pressure were kept at 25 °C and 3.4 × 10^{-6} Torr, respectively. Finally, Au source/drain electrodes were also thermally deposited on the pentacene layer by employing a shadow mask, which resulted in the TFT devices with a channel length of 100 μm and a channel width of 1000 μm.

Characterizations. Gel-permeation chromatography (GPC) was conducted on a PerkinElmer series using tetrahydrofuran as eluent and was calibrated against standard polystyrene to obtain the weight-averaged molecular weight of the SiQD−PS NC. Thermogravimetric (TG) analysis was performed on a METTLER TOLEDO SDTA851e to deduce the content of SiQD in the NC. SiQD−PS NC and PS0 samples were heated at a rate of 10 °C/min from room temperature to 800 °C in a nitrogen atmosphere. The content of the SiQD phase was obtained from the difference between the residual weights of the SiQD−PS NC and the PS0 samples. Fourier transform infrared spectroscopy (FT-IR) was performed on a PekinElmer (spectrum 400). Results were obtained after 20 scans at a resolution of 8 cm^{-1}. A SCINCO S-3150 spectrometer was used to obtain UV-vis absorption spectra of SiQD−PS NC, PS0, and octyl-capped SiQDs in the 200−1000 nm range. The spectra of solvent or quartz substrate were used as background. Photoluminescence (PL) spectra of SiQD−PS NC, PS0, and octyl-capped SiQDs were obtained upon an excitation wavelength at 325 nm by using an He−Cd light source (Kimmon Electric Co., IK3501R-G, Japan) and a photodiode array detector (IRY 102, Princeton Instrument Co., U.S.A.). Fourier-transform nuclear magnetic resonance spectroscopy was conducted on a FT-NMR 300 MHz spectrometer (Varian Inc, Palo Alto, California, U.S.A.) to obtain ^{1}H-NMR spectra of SiQD−PS NC and PS0. Transmission electron microscopy (TEM) was performed with a Tecnai G2 F30 model (FEI, Hillsboro, Oregon, USA) operated at 300 kV in a bright field mode. For TEM sampling, one drop of a solution of about 0.5 wt % of SiQD−PS NC in chlorobenzene (or a solution of 0.1 wt % of octyl-capped SiQDs in *n*-hexane) was casted onto a graphite-coated copper grid and then dried on a hot plate at 130 °C for 5 min. Cross-sectional TEM specimens were prepared through mechanical polishing followed by Ar ion milling (GATAN, PIPS 691) for electron transparency. X-ray photoelectron spectroscopy (XPS) was conducted on a MultiLab 2000 using an Mg Kα (1253.6 eV) source at a pass energy of 20 eV. For the thin film measurements, an Ar^{+} ion gun sputtering operated at

powers of 2 kV and 1.3 μA was used to clean the thin film surfaces for 2 min. Thicknesses and refractive indices of the thin films of SiQD−PS NC or PS0 were measured simultaneously by using spectroscopic ellipsometry (SE) (M2000D model, J. A. Wollam Co. Inc., U. S. A.). Cross-sectional field emission scanning electron microscope (FE-SEM) was conducted on a JSM-7500F microscope (JEOL, Asikima, Tokyo, Japan) to measure thicknesses of the pentacene channel layer and the nanocomposite layer in the TFT devices.

Charge Trapping Study. Charge trapping properties of the SiQD−PS NC were investigated from capacitance−voltage ($C-V$) characteristics obtained for the MIS devices. To measure the $C-V$ curves, an MIS device was placed on a Cu plate, which was isolated from the probe stand by a glass slice, hence placing each of the two arm tips of an HP4284 LCR meter on the Cu plate and the Al electrode. A 1 MHz AC voltage with amplitude of 1 V was applied to the top Al electrode while a DC bias was swept in the range from −25 to 15 V (forward sweep) and, conversely, from 15 to −25 V (reverse sweep). Applicability of the SiQD−PS NS as charge trapping materials in TFT based memory devices was realized through characterizations of the TFT devices whose structures are described above. The TFT characteristics including transfer and output curves were obtained on either HP1110A or HP4145B semiconductor analyzers.

3. RESULTS AND DISCUSSION

The step-wise synthesis of SiQD−PS NC and the fabrication of NC thin films on various substrates are illustrated in Scheme 1.

Scheme 1. Formation of SiQD−PS NC and the Fabrication of NC Thin Films[a]

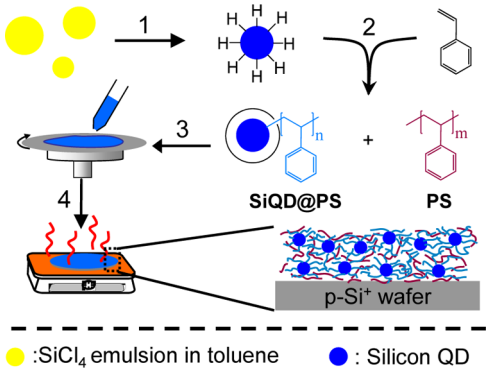

[a](1) Reducing the miniemulsion of $SiCl_4$ in toluene to H-SiQDs by $LiAlH_4$ at room temperature upon sonication; (2) refluxing the mixture of H-SiQDs and styrene for 12 h; (3) spin-coating the NC on various substrates (see text for details); (4) thermal annealing the as-coated films at elevated temperatures for 1 h in a vacuum furnace (10^{-2} Torr). Two components of the NC, polystyrene and SiQDs capped with polystyrene chains, are denoted by PS and SiQD@PS, respectively.

In step 1, pre-prepared miniemulsion of $SiCl_4$ reacted with an excess amount of $LiAlH_4$, which is a very powerful reducing agent, giving rise to hydrogen-terminated SiQDs (H-SiQDs).[22,27,28] By refluxing a mixture of H-SiQDs and styrene in step 2, both functionalization of H-SiQDs and polymerization of styrene were initiated, thus resulting in SiQDs that were terminated with polystyrene chains of different lengths (SiQD@PS) and polystyrene (PS) as follows. It is well accepted that, by thermal activation, a Si−H bond on the surfaces of H-SiQDs is homolytically cleaved, resulting in a silicon-centered radical (═SiH· or ≡S·).[24,25,29,30] An unsaturated hydrocarbon molecule, such as styrene in this study, subsequently adds to the Si radical and forms a covalent bond between the silicon atom and a carbon atom in the vinyl group of styrene; in this new configuration, the radical will position at the β-carbon atom.[29−32] This very reactive radical could either attract a hydrogen atom from neighboring Si−H groups on the QD surfaces, thus forming a silicon radical again, or propagate to form a chain radical following the addition of one styrene monomer. The newly formed Si radical started another reaction with styrene, thus leading to a high surface coverage of the SiQDs, while the propagation of the chain radical resulted in polystyrene chains of different lengths, which depend on many annihilation factors such as concentrations of monomer, impurities, and temperature. In this report, we name this type of SiQD as SiQDs capped by polystyrene chains of different lengths ($\{C_2H_3(C_6H_5)\}_n$, with $n \geq 1$) and denote by SiQD@PS whose chemical structure is cartooned in Scheme 1. The polystyrene on the surfaces of SiQDs is colored by light blue in Scheme 1.

The formation of SiQD@PS due to the surface-initiated polymerization of styrene is very similar to that of polystyrene-grafted TiO_2 nanoparticles, in which the polymerization is initiated by thermal decomposition of a initiator pre-deposited on the surfaces of TiO_2.[26] Polymerization reactions on the surfaces of H-SiQDs induced by either UV irradiation or high temperatures have been reported for other ene-functionalized monomers such as acrylic acid or triethoxyvinylsilane.[23−25] Under the synthetic conditions used in this study, thermal polymerization of styrene was also possible,[33] thus resulting in homopolystyrene component (denoted by PS and marked as violet in Scheme 1). By using GPC analysis, the weight-averaged molecular weight of this SiQD−PS NC, which contained two SiQD@PS and PS components, was estimated to be about 22 000 (Figure S1, Supporting Information). Thin films of SiQD−PS NC on various substrates were fabricated by a spin-coating method (step 3 in Scheme 1). Finally, the films were cured at different temperatures (50−300 °C) under a reduced pressure (10^{-2} Torr) (step 4 in Scheme 1) to remove the coating solvent and to test the thermal stability of the films. SiQDs are expected to disperse homogeneously in the polystyrene matrix owing to the perfect miscibility between SiQD@PS and PS.

Figure 1a shows a UV absorption spectrum of SiQD−PS NC in comparison with those of PS0 and octyl-terminated SiQDs (otc-SiQDs). While PS0 has a small absorbance above 315 nm, SiQD−PS NC and octyl-SiQDs have a very similar absorption feature with an absorption onset near 400 nm. A similar trend was also observed by comparing their photoluminescence (PL) spectra, which were obtained under an excitation wavelength at 325 nm (Figure 1b). PS0 has a minor PL efficiency compared with those of SiQD−PS NC or octyl-SiQDs. Additionally, the normalized PL spectra of SiQD−PS NC and oct-SiQDs exhibit the same feature in terms of PL maximum and emission range. These similarities between optical properties of SiQD−PS NC and oct-SiQDs indicate that the nanocomposite contained SiQDs and that the SiQDs in SiQD−PS NC and oct-SiQDs had a similar size distribution. It is because they were synthesized by post-functionalization of mother H-SiQDs, which were prepared by the same procedure. The existence of SiQDs in the nanocomposite was further confirmed by TEM and XPS analysis, shown in Figure 1c,d, respectively. In Figure 1c, SiQDs exhibit resolved lattice fringes with d-spacing of 2.7 Å, which could be attributed to the d(200) of the diamond cubic structured silicon.[34] Because of the low z-contrast of silicon over carbon, it was difficult to visualize distinctly SiQDs in the presence of polystyrene from the SiQD−PS NC sample.

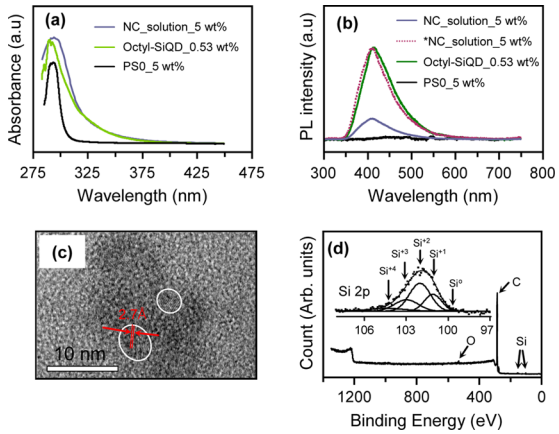

Figure 1. UV-vis absorption (a) and PL (b) spectra of SiQD−PS NC, octyl-terminated SiQDs, and PS0 in chlorobenzene solutions with indicated concentrations. In (b), "*" indicates the normalized PL spectrum (plum dotted spectrum) of SiQD−PS NC. (c) A high-resolution TEM image of SiQD−PS NC. (d) XPS survey spectrum of SiQD−PS NC; inset: Si 2p high-resolution spectrum; the experimental data (■) was fit to the dominant Si species with different oxidation states, according to ref 34.

The size and size distribution of the SiQDs in the nanocomposite were then assumed to be those of oct-SiQDs (Figure S2, Supporting Information). Therefore, the mean size in average of the SiQDs in the nanocomposite was 3.5 nm in diameter. The survey XPS spectrum of SiQD−PS NC also reveals the existence of Si phase by two low-intensity peaks with binding energies of about 101 and 152 eV, which were assigned to Si 2p and Si 2s, respectively (Figure 1d). The high-resolution XPS spectrum of Si 2p (inset in Figure 1d) exhibits a multiple-component peak at binding energy of 101.8 eV, which could originate from bulk Si−Si, surface Si−C, or sub-oxidized Si^{+}−O.[35] In this study, the binding energy of Si atoms in the SiQDs was about 101.8±0.1 eV, which is higher than that found for Si atoms in bulk silicon crystal (~99.5 eV), probably due to (1) the presence of charge trapping effect induced by irradiation that has been reported for organically passivated SiQDs,[21,35] or (2) the charging energy, the exciton Coulomb energy arising from the interaction between a photoelectron and a leaving hole, and the band-gap expansion, all of which originate from the quantum confinement effect.[36] By using TG analysis, the content of the SiQD phase in SiQD−PS NC was estimated to be 1.6 wt %, which is the difference in the residual weight between the SiQD−PS NC and PS0 samples (Figure S3, Supporting Information). By taking the densities of SiQDs and polystyrene to be 2.33 (bulk silicon) and 1.06 $g{\cdot}cm^{-3}$, respectively, the volume fraction of the SiQD phase was calculated to be 0.7 vol %. Furthermore, by using the estimated diameter of the SiQDs, of about 3.5 nm on average, density of the SiQDs in the nanocomposite was calculated to be about 3×10^{17} QDs/cm^3. IR spectrum of SiQD−PS NC is identical to that of PSO (Figure S4, Supporting Information), thus confirming the formation of polystyrene in either the SiQD@PS or the PS components as cartooned in Scheme 1. The SiQDs in the nanocomposite or the oct-SiQD sample were well passivated by polystyrene chains or octyl groups because intensities of the band in the 1000−1100 cm^{-1} range, which originates from oxidized components such as Si−O−Si or Si−OR (R═H or alkyl), were low.

The chemical structure of the nanocomposite was further characterized by NMR spectroscopy, and the result is shown in Figure 2 (blue spectrum) in comparison with that of PS0. Four

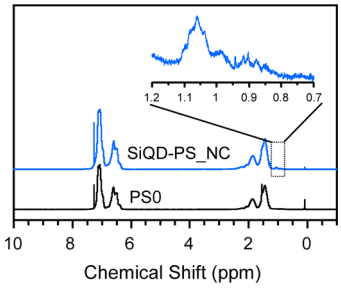

Figure 2. ^{1}H-NMR (300 MHz, $CDCl_3$) spectra of SiQD−PS NC and PS0.

proton characteristic peaks of polystyrene were observed in both samples with chemical shifts, and assignments were as follows: 1.5 ppm (═CH_2), 1.9 ppm (−CH═C), 6.5 ppm (protons at *ortho* or *para* positions of the phenyl ring), and 7.1 ppm (*metha* proton of the phenyl ring). Importantly, a low-intensive band was exclusively observed in the ^{1}H-NMR spectrum of SiQD−PS NC in the up field region from 0.8 to 1.1 ppm (see the insert in Figure 2). This band can be attributed to protons in the methylene or methyne groups next to the SiQD surfaces,[37] thus confirming the chemical bonding between polystyrene chains and SiQDs in the SiQD@PS component. Additionally, no proton peaks belonging to polycyclic aromatic compounds were observed in the down field region (chemical shift >7.4 ppm),[38] thereby supporting our previous argument that the luminescent and UV absorption properties of SiQD−PS NC originate from SiQDs.

Through the chemical characterizations and discussions above, it is demonstrated that the SiQD−PS nanocomposite contained two components: SiQDs capped by polystyrene chains of different lengths (SiQD@PS) and homopolystyrene (PS). The SiQD@PS component was produced from the thermally induced surface-initiated polymerization reaction while the PS component was formed by the thermally induced polymerization of styrene. The polystyrene chains on the surfaces of SiQDs hold multiple roles. First, they act as a potential barrier forming a spherical potential well structure for the SiQD@PS component. Second, they induce SiQD@PS to have Hansen's solubility parameters as the same as those of PS,[12] thus giving rise to a homogeneous dispersion of SiQDs in a polystyrene matrix. The third role is that they enhance the physical interactions between QDs themselves or between QDs and a polystyrene matrix. These interactions are very important to maintaining thin film morphology against stress induced by thermal annealing. For an example, spin-coated film of phenethyl-capped SiQDs was broken as soon as the coating solvent (chlorobenzene) was evaporated while that of the SiQD−PS nanocomposite was maintained smoothly even after annealing at 300 °C for 1 h in a vacuum furnace (10^{-2} Torr), (Figure S5, Supporting Information). A mixture of phenethyl-capped SiQDs and polystyrene could also give thin films having comparable morphology with those of SiQD−PS NC. Without any microscopic evidence, we think that, in the thin films of this mixture, there should be some local points at which several Si QDs are in a close proximity owing to the thinness of the phenethyl capping layer. Charge tunneling probability among these SiQDs is expected to be higher, thus causing more charge

loss, compared to the cases of SiQD−PS NC where SiQDs are separated by polystyrene chains. However, in this study, we could not optimize the length of the polystyrene chains on the surface of SiQDs because it was formed very fast, as discussed from Scheme 1, through the radical chain polymerization process. Effects of other parameters such as QD size, content of SiQDs in composite, and type of insulating matrix on the optical and electrical properties of resultant nanocomposite are still open. The synthesis of various SiQD−polymer nanocomposites by using colloidal SiQDs having vinyl or alkoxysilyl functional groups is in progress in our group to examine these issues, and the results will be reported in a separated work.

Thin films of the SiQD−PS nanocomposite were fabricated successfully on various substrates including quartz, p-Si^{+} silicon wafer, and thermally-oxidized silicon wafer (SiO_2/p-Si^{++}) by a spin-coating method, and the thin film thickness was readily tuned by changing the solution concentration or the spinning speed. The coating solvent, chlorobenzene, was completely removed under soft annealing conditions (at 50 °C and a reduced pressure of about 10^{-2} Torr). By using a coating solution with a concentration of 5 wt % and a spinning speed of 2500 (rpm), the initial thickness of the NC film on p-Si^{+} substrate was 217 nm, which is the thickness of the NC cured at 50 °C. As expected, when the curing temperature increased, the thickness of the NC film gradually decreased; these results are reported in Figure 3a. Refractive index (n) of a film, which is a

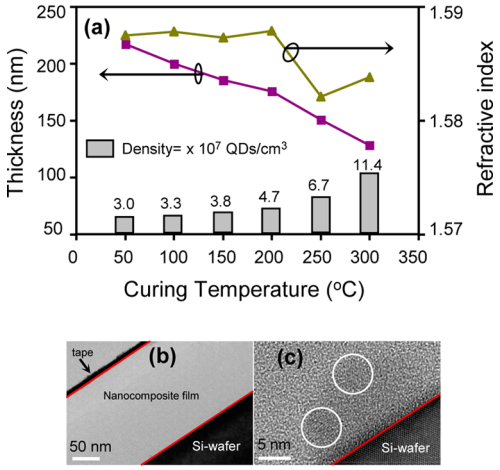

Figure 3. (a) Thicknesses (violet square), refractive indices (dark yellow triangle), and the density of SiQDs (vertical columns) of the thin films of SiQD−PS NC according to curing temperature. (b) Cross-sectional TEM image of the NC film cured at 50 °C. (c) High-resolution TEM image of the NC film cured at 50 °C. In (c), two isolated SiQDs are surrounded by white circles.

function of chemical composition and density of the film material,[10,39] can be obtained simultaneously with the film thickness through spectroscopic ellipsometry (SE) measurements.[40] The refractive indices of the NC films cured at different temperatures, determined at 633 nm, are also reported in Figure 3a. The refractive index, of about 1.588, was maintained with curing temperatures below 250 °C and slightly decreased to 1.583 by increasing the curing temperature to 250 or 300 °C. These index values are very close to those of commercial polystyrene (n = 1.587) or thin films of n-butyl-capped SiQDs.[10] This decrease, of about 0.005, in the refractive index could be attributed to the formation of nanovoids following the decomposition of polymer phase, which caused the mass lost observed in the TG curve of SiQD−PS NC (Figure S3, Supporting Information).

In addition to it, the existence of SiQDs within the NC thin films could be simply confirmed by comparing their UV absorption and PL spectra with those of PS0 films (see Figure S6, Supporting Information). The density of SiQDs in the NC film, indicated by vertical columns in Figure 3a, increased gradually from 3 × 10^7 to 11.4 × 10^7 QDs/cm^3 because the polystyrene phase was decomposed by high curing temperatures (Figure S3, Supporting Information).

We have discussed above that SiQDs can be homogeneously dispersed in polystyrene matrix in the SiQD−PS nanocomposite owing to the polystyrene chains on the surface of SiQDs in the SiQD@PS component. To support this argument, cross-sectional TEM was conducted for three representative NC films cured at 50, 150, and 250 °C; the results are shown in Figures 3b and S7 (Supporting Information), respectively. Low-magnification TEM images appear smoothly gray, (see Figure 3b), probably due to the low content of the SiQD phase (about 1.6 wt % or 0.7 vol %), the low atomic number Z-contrast of silicon, and the absence of QD aggregations in the film. If SiQDs aggregated during the thin film processing, the aggregates would cumulatively scat the transmitting electrons, thus resulting in some darker regions in the TEM images, which were not observed in Figures 3b and S7 (Supporting Information). In a high-magnification TEM image (Figure 3c), one could see some SiQDs that are far away from each other and from the substrate owing to the polystyrene chains on the QD surfaces.

As we have discussed and cartooned in Scheme 1, the SiQD@PS component realizes a spherical potential well structure, in which the SiQD and its capping layer composed of polystyrene chains act as a well and a potential barrier, respectively. Very similar to the well characterized SiQDs embedded in metal oxides, SiQD−PS NC is expected to have charge trapping and de-trapping abilities. The charge trapping properties of a dielectric material can be investigated conveniently through its capacitance−voltage (C−V) characteristics for a MIS device.[39,41,42] It will be discussed below that positive charges (holes) are controllably injected to, stored in, or ejected from the SiQDs dispersed in the NC films.

C−V curves of the thin films of SiQD−PS NC or PS0 cured at different temperatures obtained through their corresponding MIS devices, whose structure is schematically illustrated in Figure 4a, are summarized in Figure 4b−h. Please remember that PS0 was synthesized by using the same procedure for the synthesis of SiQD−PS NC, except for the addition of $SiCl_4$. The C−V curve of the PS0 film exhibits a minor hysteresis (Figure 3h) while those of the SiQD−PS NC films display a well-defined counterclockwise hysteresis (Figure 3b−g). Since PS0 can be regarded as the PS component of SiQD−PS NC, the C−V hysteresis is safely attributed to the presence of the SiQD@PS component in the nanocomposite. More concretely, because the flat band voltages were negative, the C−V hysteresis is due to the hole trapping to and de-trapping from SiQDs within the NC films.[16,39,42]

In a MIS device, charge trapping and de-trapping behaviors of the NC films can be closely related to energy levels of the SiQDs with respect to the others. Figure 5 shows the energy diagram of the MIS devices used in this study. Polystyrene is a wide-bandgap insulator, whose highest occupied molecular orbital (HOMO) and the lowest unoccupied molecular orbital (LUMO) energy levels are about −7 and −3 eV with respect to

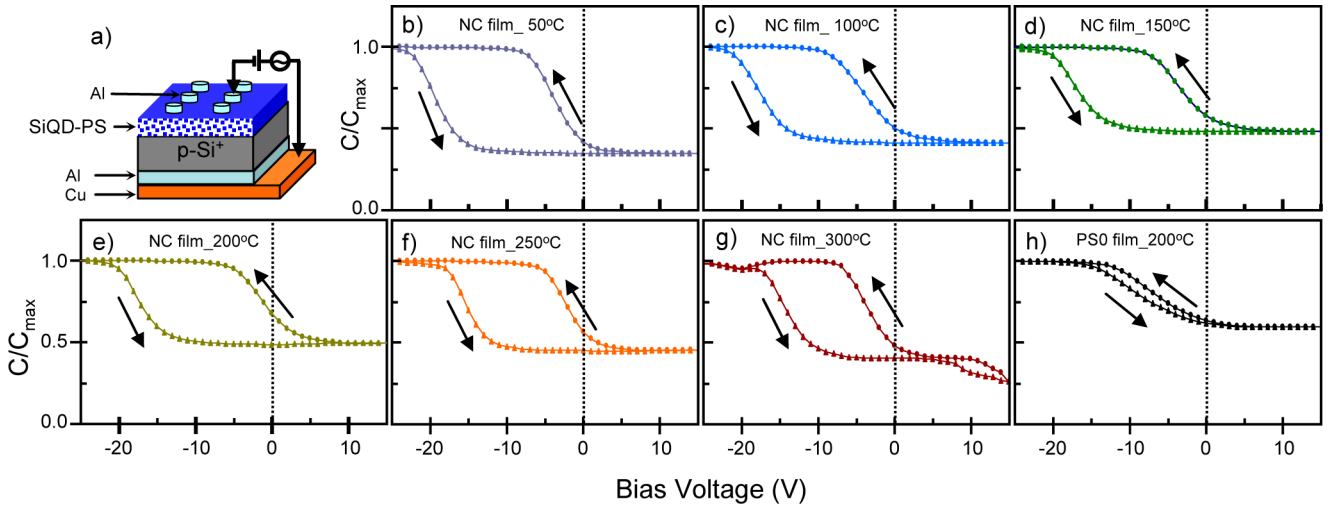

Figure 4. (a) Illustration of the $C-V$ measurement for an Al/SiQD−PS NC film/p-Si$^+$ MIS device. (b−g) $C-V$ curves for the NC films, which were cured at different temperatures (inset). (h) $C-V$ curve for the PS0 film cured at 200 °C.

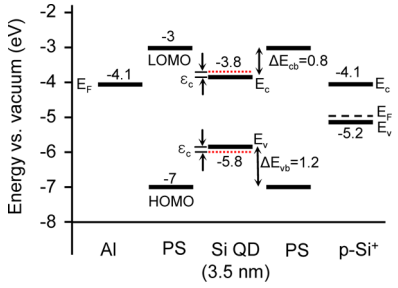

Figure 5. Energy diagram of the MIS device.

the vacuum level, respectively.[43] Energy levels of the valence band edge (E_v), the Fermi (E_F), and the conduction band edge (E_c) of p-type silicon, respectively, are −5.2, −5.0, and −4.1 eV.[44] The Fermi energy level of Al is known to be −4.1 eV.[44] Energy gap of a 3.5 nm SiQD is about 2 eV;[45] the diameter of 3.5 nm is the average size of SiQDs as estimated from a control sample, octyl-capped SiQDs (Figure S2, Supporting Information). By assuming that the quantum confinement effect causes valence band shift equal to twice of the conduction band shift,[46] the E_c and E_v of the 3.5 nm SiQD were estimated to be −5.8 and −3.8 eV, respectively. The valence band (conduction band) offset, ΔE_{vb} (ΔE_{cb}), of the SiQDs embedded in polystyrene, which is defined as the difference between the valence band (conduction band) edge of the SiQD and HOMO (LUMO) of polystyrene, was calculated to be 1.2 eV (0.8 eV). This ΔE_{vb} (ΔE_{cb}) is the height of the potential barrier for hole (electron), thus defining the spherical potential well that we have mentioned throughout this report for the SiQD@PS component of the SiQD−PS nanocomposite. Another factor that can greatly influence the charging behavior of SiQDs is charging energy (ε_c),[42] which is defined as the energy needed to add an additional electron on the QD. In the simplest form,

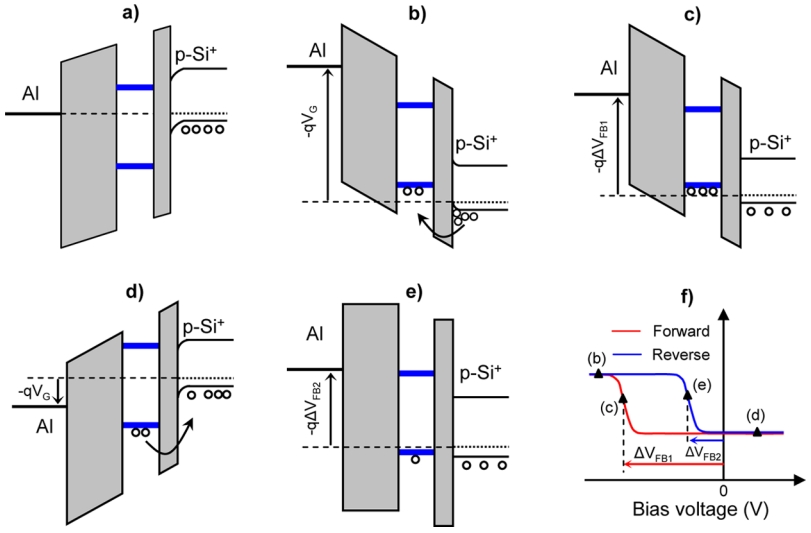

Figure 6. Energy band diagram of an MIS structure under different bias condition: (a) contact; (b) negative bias voltage corresponding to accumulation mode; (c) bias at flat band voltage in the forward scan; (d) positive bias voltage; (e) bias at flat band voltage in the reverse scan; (f) $C-V$ behavior with bias condition in panels a−e. For simplicity, only HOMO and LUMO of a 3.5 nm SiQD are shown and indicated by horizontal blue lines. The HOMO−LUMO gap of polystyrene is represented by gray bars. Holes (indicated by open circles) are injected to, stored in, and ejected from the SiQD in panels b, c, and d, respectively. No or very few holes are stored in panel e.

dx.doi.org/10.1021/am400356r | ACS Appl. Mater. Interfaces 2013, 5, 2400−2409

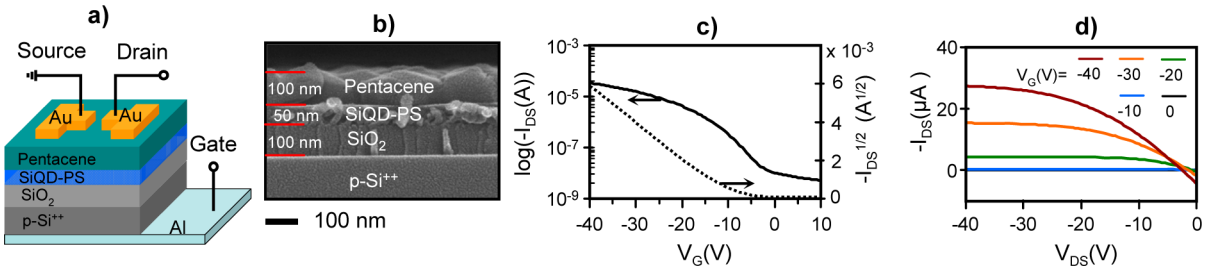

Figure 7. (a) Schematic structure, (b) cross-section SEM image, (c) transfer curve (V_{DS} = −40 V), and (d) output characteristics of the p-Si^{++}/SiO$_2$/NC film cured at 200 °C/pentacene/Au source-drain TFT device.

charging energy is reversely proportional to the QD diameter (d) and dielectric constant of the surrounding medium (ε_m = 2.7 for polystyrene): $\varepsilon_c = e^2/(4\pi d\varepsilon_0\varepsilon_m)$,[8] where e is the fundamental unit of charge; $\varepsilon_0 = 8.85 \times 10^{-12}$ (F·m^{-1}) is the permittivity of a vacuum. By using this equation, the charging energy of a 3.5 nm SiQD in polystyrene matrix was calculated to be 0.15 eV; this value is consistent with the charging energy reported for a 3.5 nm SiQD surrounded by SiO$_2$ (ε_m = 3.9 for SiO$_2$), of about 0.09 eV, measured by scanning tunneling spectroscopy.[45] By taking this charging energy into account, the effective barrier height for hole (electron) reduces to be 1.05 eV (0.65 eV) for the first trapped hole (electron), as depicted by red dotted lines in Figure 5. As a result of it, hole trapping in the nanocomposite films, which caused the $C-V$ hysteresis in Figure 4b−g, is surely more pronounced than electron trapping due to its larger effective barrier height.[42]

The hole trapping to, storing in, and de-trapping from SiQDs, which caused the $C-V$ hysteresis observed in Figure 4b−g, can be concisely explained as follows. Upon tip contacting to the Al electrode and the p-Si$^+$ substrate, their Fermi energy levels aligns (Figure 6a); the HOMO and LUMO energy levels of polystyrene adjust accordingly with respecting to their vacuum levels.[44] When applying a large negative bias voltage (V_G) to the Al electrode (Figure 6b), the bands of p-Si$^+$ were bent upward and a hole accumulation layer appeared at the polystyrene−p-Si$^+$ interfaces, from which holes were injected into the valence band states (herein, for clarity purposes, only HOMO is shown) of SiQDs. The first six holes added to a SiQD will occupy the 6-fold degenerate states at the top of the valence band;[47] thereby, they have the sample energy levels. The number of trapped holes represented in Figure 6 is only for relative comparison; it does not indicate an actual value. Because the charging energy, of about 0.15 eV, is much larger than the thermal energy (k_BT, where k_B and T are Boltzmann constant and absolute temperature) at room temperature, of about 0.026 eV, hole injection into a SiQD was not continuous but was cost by a hole−hole Coulomb energy, which is in the order of charging energy (0.15 eV),[47] for each added hole. Consequently, the effective energy level of trapping state decreased stepwisely by 0.15 eV, or in other words, the effective potential barrier for trapped hole decreased. Nayfeh and co-workers reported that an effective barrier of 0.5 eV is not sufficient for electron trapping.[42] If one assumed that 0.5 eV was a lower limit for charge trapping, one electron or four holes could be trapped in a SiQD in our system. Due to the presence of trapped holes in the nanocomposite film after applying a negative bias, the flat band voltage (ΔV_{FB1}), at which the bands of p-Si$^+$ are flat, was negative (Figure 6c).[39] When a positive bias voltage was applied to Al, the bands of p-Si$^+$ were bent downward and a depletion region appeared at the polystyrene−p-Si$^+$ interfaces following the energy levels of Al and valence band states of SiQD adjustments;[44] thereby, the trapped holes were forcibly ejected from SiQDs to p-Si$^+$ (Figure 6d), thus resulting in no or very few holes maintained in the nanocomposite film (Figure 6e). Because the density of trapped charges is directly proportional to the flat band shift,[39] the fewer number of trapped holes in the reverse scan gave the smaller flat band shift ($\Delta V_{FB2} < \Delta V_{FB1}$), thus giving rise to a counterclockwise $C-V$ hysteresis that was observed in Figure 4b−g or schematically shown in Figure 6f.

It is demonstrated that holes were controllably injected to or ejected from thin films of the nanocomposite sandwiched in MIS devices by tuning a negative bias stress ($-V_G$) or a positive bias stress ($+V_G$), respectively, (Figure S8, Supporting Information). After applying a bias stress to Al electrode for about 5 s, $C-V$ curves were obtained for a film cured at 50 °C by scanning the bias voltage in the range from −13 to 7 V; this range was chosen so that the trapped holes could not be ejected (no $C-V$ hysteresis). When the $-V_G$ increased, the flat band voltage shifted to the left side, indicating that more holes were forcibly injected into the NC film (Figure S8a, Supporting Information). Meanwhile, trapped holes, which were initially charged in the NC film by applying a −40 V bias stress to Al electrode, were ejected more and more by increasing the $+V_G$, as indicated by the right-shifting of the flat band voltage (Figure S8b, Supporting Information). Additionally, electron trapping to the NC was feasible, indicated by a positive flat band voltage, if highly positive bias stress was used, such as 40 V (Figure S8b, Supporting Information).

To turn back to Figure 4, it is notable that $C-V$ characteristics for the thin films of SiQD−PS NC were almost the same over a wide range of curing temperatures, from 50 to 250 °C (see Figure 4b−f). We could not find any direct relation between the width of the $C-V$ hysteresis and the density of SiQDs within the NC film (Figure 3a). Likely, the hole injection/ejection that has been discussed from Figure 6 was restricted to SiQDs near the p-Si$^+$ semiconductor. In this circumstance, the polystyrene chains on the surfaces of SiQDs are very important because they do not only act as a barrier layer to confine the trapped holes but also, in the case of intimate contact to p-Si$^+$, work as a tunneling layer through which holes inject to or eject from the QDs. Upon curing at 300 °C, the $C-V$ curve slightly changed at high positive bias voltages (Figure 4g). Because FT-IR and X-ray photoelectron spectroscopy (XPS) Si 2p spectra of the NC thin film was maintained at high curing temperatures (Figures S9 and S10, Supporting Information), an accurate chemical origin accounting for the change in $C-V$ curves for the NC film cured at 300 °C was still lacking. Possibly, at high curing temperatures, the Si−C bonds between SiQDs and their capping polystyrene

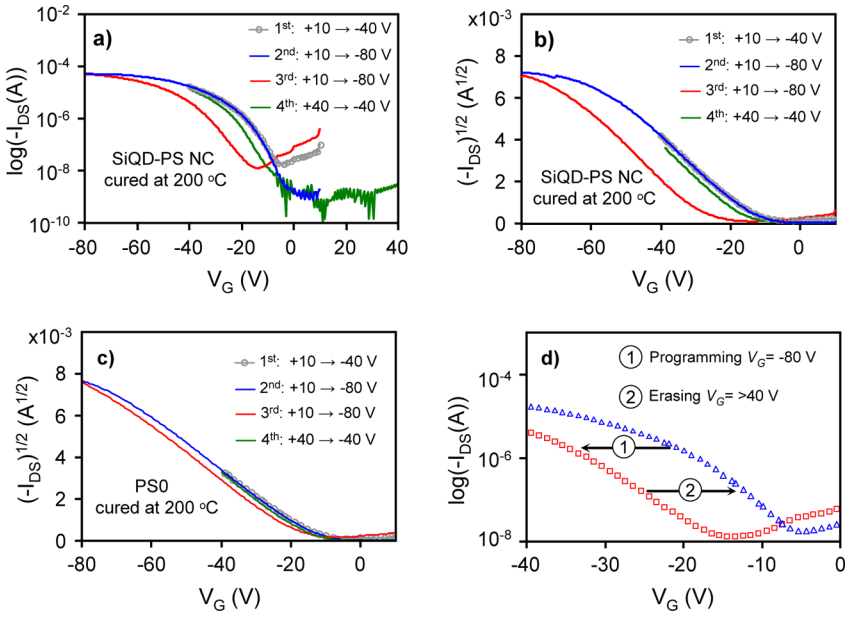

Figure 8. (a) Transfer curves and (b) plots of root square of I_{DS} vs. V_G obtained from different scans for the TFT devices using films of SiQD−PS NC cured at 200 °C. (c) Plots of root square of I_{DS} vs. V_G for the control TFT device using a film of PS0 cured at 200 °C. (d) The 1st and 3rd transfer curves taken from (a) and shown in a V_G range from −40 to 0 V with assumptions that the hole injection was induced by a V_G at −80 V and that the hole ejection was completed by a V_G > 40 V. The I_{DS} data was obtained by scanning V_G four consecutive times with respective V_G ranges that are indicated in (a−c), and a V_{DS} = −40 V was used.

chains were cleaved, thus ruining the spherical potential well structure of the SiQD@PS component. One line of evidence for this argument is the PL quenching observed in the NC film cured at 300 °C, which could be attributed to the formation of Si dangling bonds on the surface of SiQDs (Figure S6, Supporting Information).

In order to realize the applicability of the SiQD−PS nanocomposite into OTFT based memory devices, TFT devices having a structure of p-Si^{++}/SiO_2/NC film/pentacene/Au source-drain were fabricated using a thin film of the NC on the SiO_2/p-Si^{++} substrate cured at 200 °C. This curing temperature is suitable for most of the flexible substrates, and it is high enough to test the thermal stability of the NC. Two control TFT devices with a structure of p-Si^{++}/SiO_2/with or without a thin film of PS0/pentacene/Au source-drain were also fabricated for comparison. The commercially available thermally-oxidized silicon wafer (SiO_2/p-Si^{++}) has a 100 nm thick SiO_2 layer deposited on the surfaces of low-resistivity p-Si^{++} wafer; this SiO_2 layer served as a buffer layer in the TFTs used in this study.[48] Backside of the p-Si^{++} substrate was deposited with a thin layer of Al metal and served as a back gate. The structure of these TFTs is schematically shown in Figure 7a. Thicknesses of the SiO_2, SiQD−PS nanocomposite, and pentacene layers were determined by cross-sectional SEM to be about 100, 50, and 100 nm, respectively (Figure 7b). Transfer (Figure 7c) and output curves (Figure 7d) of the TFT device using SiQD−PS NC exhibit the p-channel TFT characteristics; a cross-section SEM image, transfer curves, and output characteristics of the control TFTs are shown in Figures S11 and S12 (Supporting Information). From the conventional characterization equations,[49] values of mobility (μ), threshold voltage (V_{th}), and I_{on}/I_{off} ratio for the TFT device using the NC were calculated to be 0.34 ($cm^2V^{-1}s^{-1}$), −9.5 V, and 7.4×10^3, respectively; these values are comparable to those of a control TFT device using PSO. Notably, the use of NC improved significantly the mobility and I_{on}/I_{off} ratio when compared with those of the p-Si^{++}/SiO_2/pentacene/Au TFT device (Table S1, Supporting Information), because of the hydrophobicity of the NC layer.[17]

The above TFT properties were performed on an HP4145B semiconductor analyzer with a gate voltage (V_G) limited to 40 V (from −40 V to +40 V), which was not sufficient to cause charge injection from the pentacene channel layer to the nanocomposite layer; thereby, the expected memory characteristics, which are directly indicated by a shift in the transfer curve, were not observed. An HP1110A semiconductor analyzer was then employed because it can provide V_G in a wider range, from −80 V to +80 V. For each TFT device using either film of SiQD−PS NC or film of PS0 cured at 200 °C, the drain current (I_{DS}) was obtained from four consecutive scans by applying a drain voltage (V_{DS}) at −40 V to the source-drain while V_G was allowed to sweep, respectively, from 10 to −40 V for the first scan (denoted by "1st: 10 → −40 V"), from 10 to −80 V for the second scan (2nd: 10 → −80 V), from 10 to −80 V for the third scan (3rd: 10 → −80 V), and from 40 to −40 V for the fourth scan (4th: 40 → −40 V). These results are summarized in Figure 8a−c.

The transfer curve for the TFT device using SiQD−PS NC obtained by scanning V_G from 10 to −40 V (the first scan, gray-circled curve in Figure 8a) was identical to that shown in Figure 7c, indicating that the TFT characteristics were reproducible. It is clear from Figure 8a that the transfer curve was shifted by changing the V_G range and scanning sequence. No shift in the transfer curve was observed between the second and the first scans while a well-defined negative shift was observed between the third and second scans (Figure 8a). Then, the transfer curve turned back almost to the initial state, which is defined by the first scan. Correspondingly, V_{th} shifted from −12 V (in the first or the second scans) to −27 V (in the third scan) and then turned back to −15 V (in the fourth scan), Figure 8b. By using the same measurement procedure, V_{th} obtained on a control TFT device using PS0 shifted from −13 V (in the first or the

second scans) to −16 V (in the third scan) and then turned back to −13 V (in the fourth scan), Figure 8c. Therefore, the large shifts in the transfer curve or V_{th} observed in Figure 8a,b were surely attributed to the SiQD@PS component of the nanocomposite. These shifts, which responded to the V_G range and scanning sequence, can be fairly explained by the hole trapping ability of the NC that we have discussed through Figures 4−6, as follows. A band diagram for the p-Si^{++}/SiO_2/SiQD−PS NC/pentacene/Au TFT device is shown in Figure S13 (Supporting Information), which is similar to that of the MIS device shown in Figure 5. By applying a highly negative V_G, such as −80 V, in the second scan, holes were forcibly injected from an accumulation layer developed at the NC−pentacene interfaces into SiQDs within the NC layer. The trapped holes maintained in the NC layer, which were not ejected by a low positive V_G (<10 V) in the third scan, effectively reduced the electric field across the device thickness, thus shifting the transfer curve to the negative direction compared to that in the second scan. Holes were absent in the NC layer after the first scan, as indicated by no transfer curve shifting between the second and the first scans (Figure 8a). We think the thick SiO_2 buffer layer, whose thickness was 100 nm, reduced the applied field, which is the driving force for the hole injection from the p-channel to the NC trapping layer so that with V_G of about −40 V in the first scan was not sufficient to cause the hole injection. By applying a highly positive V_G, such as +40 V, in the fourth scan, the trapped holes were partially ejected, thus resulting in a fewer amount of trapped holes maintained in the NC layer. As a result of it, the transfer curve turned back almost to the initial state where no holes were present.

Figure 8d shows two representative transfer curves that were obtained from the first and the third scans; thereby, memory characteristics are realized if one assumes the hole injection to and hole complete ejection from the SiQDs by applying, respectively, a V_G at −80 V (programming) or a V_G > +40 V (erasing). The difference in drain current between the two states was about 2 orders of magnitude (see Figure 8d).

An additional TFT device using a NC on SiO_2/p-Si^{++} film cured at 100 °C was fabricated in an effort to study the effects of Si QD density and thickness of NC layer on the FET memory characteristics, although the curing temperature does not likely cause significant change in the trapping ability of NC, Figure 4b−g. TFT characteristics and memory behavior of this device are summarized in Figure S14 (Supporting Information). As expected, this device also exhibits FET memory behaviors, resembling those shown in Figure 8a,b for the TFT device involving a NC layer cured at 200 °C, with an exception that the width of transfer curve hysteresis, which is an indicator of charge trapping density, is smaller, 10 vs. 15 V. Despite lower QD density in the NC layer, 3.3×10^7 vs. 4.7×10^7 (dots/cm^3), the origin of smaller transfer curve hysteresis (10 V) is not likely, because the QD density trivially affects charge trapping density, Figure 4b−g. This variation may be due to a lower carrier concentration in the pentacene layer, as indicated by the lower mobility (0.11 vs. 0.36 $cm^2V^{-1}s^{-1}$; Figure S14a and Table S1, Supporting Information).[50] More studies relating to the synthesis of Si QD based nanocomposites with a controllable Si QD content and device engineering are needed to understand the effects of Si QD composition as well as the thickness of charge trapping layer on the FET memory characteristics. Such kinds of experiments have been carried out in our laboratory, and the results will be communicated in a separate report.

In conclusion, we have demonstrated the synthesis of SiQD−PS nanocomposite through a thermally-induced surface-initiated polymerization approach using pre-prepared hydrogen-terminated SiQDs. The nanocomposite consisted of two miscible components: SiQD@PS and PS which, respectively, are SiQDs capped by polystyrene chains and homopolystyrene formed simultaneously. SiQD@PS component has a spherical potential well structure in which a SiQD and polystyrene chains on its surfaces act as a well and a potential barrier, respectively. Through a study on MIS devices using thin films of this nanocomposite cured at different temperatures, it has been demonstrated that the spherical potential well accounted for the hole trapping and de-trapping abilities of the NC and the strong covalent bonds between the SiQDs and the polystyrene chains were responsible for the thermal stability of these abilities. Transfer curves obtained for an OTFT based memory device, that employed the SiQD−PS nanocomposite as a trapping material and pentacene as a channel layer, were controllably shifted by changing gate voltage, thus realizing the memory characteristics. Importantly, in this study, thin films of the nanocomposite that exhibited charge trapping properties were fabricated by using a solution process and low curing temperatures; these conditions are suitable for large-scale and flexible device fabrications. We think that this study is a starting point for a new type of silicon quantum dot based nanocomposite for solution-processed nonvolatile memory applications. Further study investigating effects of the dielectric constant of the insulating matrix, size of SiQDs, and density of SiQDs in the nanocomposite and more precise memory characterizations are needed to optimize the use of this nanocomposite.

■ ASSOCIATED CONTENT

Ⓢ Supporting Information

Additional Table S1 and Figures S1−14. This material is available free of charge via the Internet at http://pubs.acs.org.

■ AUTHOR INFORMATION

Corresponding Author

*E-mail: hdjeong@chonnam.ac.kr. Tel: +82-62-530-3387. Fax: 82-62-530-3388.

Notes

The authors declare no competing financial interest.

■ ACKNOWLEDGMENTS

This research was supported by the Basic Science Research Program through the National Foundation of Korea (NRF) funded by the Ministry of Education, Science and Technology (No. 2010-0008824). This research was also supported by the Basic Science Research Program through the National Research Foundation of Korea (NRF) funded by the Ministry of Education, Science and Technology (No. 2012R1A1A2039579).

■ REFERENCES

(1) Tiwari, S.; Rana, F.; Hanafi, H.; Hartstein, A.; Crabbé, E. F.; Chan, K. *Appl. Phys. Lett.* **1996**, *68*, 1377−1379.

(2) Choi, W. K.; Chim, W. K.; Heng, C. L.; Teo, L. W.; Ho, V.; Ng, V.; Antoniadis, D. A.; Fitzgerald, E. A. *Appl. Phys. Lett.* **2002**, *80*, 2014−2016.

(3) Yun, D. Y.; Son, J. M.; Kim, T. W.; Kim, S. W.; Kim, S. W. *Appl. Phys. Lett.* **2011**, *98*, 243306.
(4) Tsoukalas, D.; Dimitrakis, P.; Kolliopoulou, S.; Normand, P. *Mater. Sci. Eng. B* **2005**, *124*, 93−101.
(5) Oda, S.; Huang, S. In *Silicon Nanocrystals: Fundamentals, Synthesis and Applications*; Pavesi, L., Turan, R., Eds.; Wiley-VCH Verlag GmbH & Co. KGaA: Weiheim, Germany, 2010; Vol. *15*, p 395−444.
(6) Gelinck, G. *Nature* **2007**, *445*, 268−270.
(7) Lee, J. S.; Kim, Y. M.; Kwon, J. H.; Shin, H.; Sohn, B. H.; Lee, J. *Adv. Mater.* **2009**, *21*, 178−183.
(8) Kim, S. J.; Lee, J. S. *Nano Lett.* **2010**, *10*, 2884−2890.
(9) Chen, Y. C.; Huang, C. Y.; Yu, H. C.; Su, Y. K. *J. Appl. Phys.* **2012**, *112*, 034518.
(10) Choi, J. K.; Jang, S.; Sohn, H.; Jeong, H. D. *J. Am. Chem. Soc.* **2009**, *131*, 17894−17900.
(11) Dung, M. X.; Mohapatra., P.; Choi, J. K.; Kim, J. H.; Jeong, S.; Jeong, H. D. *Bull. Korean Chem. Soc.* **2012**, *33*, 1491−1504.
(12) Barton, A. F. M. *CRC Handbook of Polymer-Liquid Interaction Parameters and Solubility Parameters*; CRC Press, Inc: Boca Raton, Florida, 1990; Vol. *1*, p 11; Vol. *2*, p 297.
(13) Ouyang, J.; Chu, C. W.; Szmanda, C. R.; Ma, L.; Yang, Y. *Nat. Mater.* **2004**, *31*, 918−922.
(14) Liu, C. L.; Hsu, J. C.; Chen, W. C.; Sugiyama, K.; Hirao, A. *ACS Appl. Mater. Interfaces* **2009**, *1*, 1974−1979.
(15) Hwang, S. K.; Lee, J. M.; Kim, S.; Park, J. S.; Park, H. I.; Ahn, C. W.; Lee, K. J.; Lee, T.; Kim, S. O. *Nano Lett.* **2012**, *12*, 2217−2221.
(16) Leong, W. L.; Lee, P. S.; Lohani, A.; Lam, Y. M.; Chen, T.; Zhang, S.; Dodabalapur, A.; Mhaisalkar, S. G. *Adv. Mater.* **2008**, *20*, 2325−2331.
(17) Yang, H.; Kim, S. H.; Yang, L.; Yang, S. Y.; Park, C. E. *Adv. Mater.* **2007**, *19*, 2868−2872.
(18) Hessel, C. M.; Reid, D.; Panthani, M. G.; Rasch, M. R.; Goodfellow, B. W.; Wei, J.; Fujii, H.; Akhavan, V.; Korgel, B. A. *Chem. Mater.* **2012**, *24*, 393−401.
(19) Shirahata, N.; Hasegawa, T.; Sakka, Y.; Tsuruoka, T. *Small* **2010**, *6*, 915−921.
(20) Veinot, J. G. C. *Chem. Commun.* **2006**, 4160−4168.
(21) Dung, M. X.; Tung, D. D.; Jeong, S.; Jeong, H. D. *Chem. Asian J.* **2013**, *8*, 653−664.
(22) Tilley, R. D.; Warner, J. H.; Yamamoto, K.; Matsui, I.; Fujimori, H. *Chem. Commun.* **2005**, 1833−1835.
(23) Guan, M.; Wang, W.; Henderson, E. J.; Dag, Ö.; Kübel, C.; Chakravadhanula, V. S. K.; Rinck, J.; Moudrakovski, I. L.; Thomson, J.; McDowell, J.; Powel, A. K.; Zhang, H.; Ozin, G. A. *J. Am. Chem. Soc.* **2012**, *134*, 8439−8446.
(24) Clark, R. J.; Dang, M. K. M.; Veinot, J. G. C. *Langmuir* **2010**, *26*, 15657−15664.
(25) Rogozhina, E. V.; Eckhoff, D. A.; Gratton, E.; Braun, P. V. *J. Mater. Chem.* **2006**, *16*, 1421−1430.
(26) Matsuno, R.; Otsuka, H.; Takahara, A. *Soft Mater* **2006**, *2*, 415−421.
(27) Wilcoxon, J. P.; Samara, G. A.; Provencio, N. P. *Phys. Rev. B* **1999**, *60*, 2704−2714.
(28) Wang, J.; Sun, S.; Peng, F.; Cao, L.; Sun, L. *Chem. Commun.* **2011**, *47*, 4941−4943.
(29) Sieval, A. B.; Linker, R.; Zuilhof, H.; Sudhölter, E. J. R. *Adv. Mater.* **2000**, *12*, 1457−1460.
(30) Buriak, J. M. *Chem. Rev.* **2002**, *102*, 1271−1308.
(31) Jariwala, B. N.; Dewey, O. S.; Stradins, P.; Ciobanu, C. V.; Agarwal, S. *ACS Appl. Mater. Interfaces* **2011**, *3*, 3033−3041.
(32) Weeks, S. L.; Bart, M.; van de Sanden, M. C. M.; Agarwal, S. *Langmuir* **2012**, *28*, 17295−17301.
(33) Hui, A. W.; Hamielec, A. E. *J. Appl. Polym. Sci.* **1972**, *16*, 749−769.
(34) Yerci, S.; Doğan, I.; Seyhan, A.; Gencer, A., Turan, R. In *Silicon Nanocrystals: Fundamentals, Synthesis and Applications*; Pavesi, L., Turan, R., Eds.; Wiley-VCH Verlag GmbH & Co. KGaA: Weiheim, Germany, 2010; Vol. *21*, p 598.
(35) Chao, Y.; Krishnamurthy, S.; Montalti, M.; Lie, L. H.; Houlton, A.; Horrocks, B. R.; Kjeldgaard, L.; Dhanak, V. R.; Hunt, M. R. C.; Šiller, L. *J. Appl. Phys.* **2006**, *98*, 044316.
(36) Cheng, T. P.; Liu, Y.; Sun, C. Q.; Tse, M. S.; Hsieh, J. H.; Fu, Y. Q.; Liu, Y. C.; Fung, S. *J. Phys. Chem. B* **2004**, *108*, 16609−16612.
(37) Hua, F.; Erogbogbo, F.; Swihart, M. T.; Ruckenstein, E. *Langmuir* **2006**, *22*, 4363−4370.
(38) Lee, H. M.; Kim, Y. N.; Kim, B. H.; Kim, S. O.; Cho, S. O. *Adv. Mater.* **2008**, *20*, 2094−2098.
(39) Choi, J. K.; Jang, S.; Kim, K. J.; Sohn, H.; Jeong, H. D. *J. Am. Chem. Soc.* **2011**, *133*, 7764−7785.
(40) Tompkins, H. G.; McGahan, W. A. *Spectroscopic Ellipsometry and Reflectometry*; John Wiley-Interscience: New York, 1999; Vol. *8*, p 88.
(41) Gupta, R. K.; Kusuma, D. Y.; Lee, P. S.; Srinivasan, M. P. *ACS Appl. Mater. Interfaces* **2011**, *3*, 4619−4625.
(42) Nayfeh, O. M.; Antoniadis, D. A.; Mantey, K.; Nayfeh, M. H. *Appl. Phys. Lett.* **2007**, *90*, 153105.
(43) Duke, C. B.; Fabish, T. J. *Phys. Rev. Lett.* **1976**, *37*, 1075−1078.
(44) Barbottin, G.; Simonne, J. J.; Vapaille, A. In *Instabilities in Silicon Devices*; Barbottin, G., Vapaille, A., Eds.; Elsevier Science Publisher B.V: Amsterdam, 1991; Vol. *1*, Chapter 4, pp 223−262.
(45) Zaknoon, B.; Bahir, G.; Saguy, C.; Edrei, R.; Hoffman, A.; Rao, R. A.; Muralidhar, R.; Chang, K. M. *Nano Lett.* **2008**, *8*, 1689−1694.
(46) van Buuren, T.; Dinh, L. N.; Chase, L. L.; Siekhaus, W. J.; Terminello, L. J. *Phys. Rev. Lett.* **1998**, *80*, 3803−3806.
(47) Franceschetti, A.; Zunger, A. *Phys. Rev. B* **2000**, *62*, 2614−2623.
(48) Baeg, K. J.; Noh, Y. Y.; Ghim, J.; Kang, S. J.; Lee, H.; Kim, D. Y. *Adv. Mater.* **2006**, *18*, 3179−3183.
(49) Zaumseil, J.; Sirringhaus, H. *Chem. Rev.* **2007**, *107*, 1296−1323.
(50) Tanase, C.; Meijer, E. J.; Blom, P. W. M.; de Leeuw, D. M. *Phys. Rev. Lett.* **2003**, *91*, 216601.